Liquid Crystals
Publication details, including instructions for authors and subscription information:
http://www.informaworld.com/smpp/title~content=t713926090

Synthesis and phase behaviour of new cholesteric monomers and side chain smectic polymers based on cholesterol

Jian-She Hu[a]; Li-Qun Yang[a]; Xia Zhang[a]; Zhi-Wei Song[a]
[a] Center for Molecular Science and Engineering, College of Science, Northeastern University, Shenyang, People's Republic of China

Online publication date: 20 October 2010

To cite this Article Hu, Jian-She , Yang, Li-Qun , Zhang, Xia and Song, Zhi-Wei(2010) 'Synthesis and phase behaviour of new cholesteric monomers and side chain smectic polymers based on cholesterol', Liquid Crystals, 37: 10, 1259 — 1268
To link to this Article: DOI: 10.1080/02678292.2010.497229
URL: http://dx.doi.org/10.1080/02678292.2010.497229

Liquid Crystals,
Vol. 37, No. 10, October 2010, 1259–1268

Taylor & Francis
Taylor & Francis Group

Synthesis and phase behaviour of new cholesteric monomers and side chain smectic polymers based on cholesterol

Jian-She Hu*, Li-Qun Yang, Xia Zhang and Zhi-Wei Song

Center for Molecular Science and Engineering, College of Science, Northeastern University, Shenyang, People's Republic of China

(*Received 27 December 2009; final version received 26 May 2010*)

The synthesis of five new cholesteryl-based monomers (**M-1**–**M-5**) and the corresponding smectic comb-like polymers containing cholesteryl groups (**P-1**–**P-5**) is presented. The chemical structures were characterised by FT-IR, 1H NMR and elemental analyses. The specific optical rotations were evaluated with a polarimeter. The phase behaviour was investigated by polarising optical microscopy, differential scanning calorimetry, thermogravimetric analysis, and X-ray diffraction. The specific optical rotation values of these monomers and polymers with the same number of phenyl rings and terminal groups were nearly equal; however, they decreased with increasing the aryl numbers in the mesogenic core. The monomers **M-1**–**M-5** showed oily streak and focal conic optical textures, or finger print textures characteristic of the chiral nematic phase. The polymers **P-1**–**P-5** showed the smectic A phase. The melting, clearing, and glass transition temperatures increased, and the mesophase temperature ranges widened with increasing the aryl number in the mesogenic core. However, although the molecular structures of **M-4** and **M-5** were similar to those of **M-3**, namely their mesogenic cores contained three phenyl rings, their phase behaviour differed considerably, and T_m and T_i of **M-4** and **M-5** were less than those of **M-3**. In addition, **M-4** and **M-5** showed a clear glass transition similar to the polymer. Furthermore, the ester linkage bond and aryl arrangement in the mesogenic core also affected the phase behaviour.

Keywords: liquid crystalline polymers; phase behaviour; cholesteric phase; smectic A phase; chiral

1. Introduction

Both from a scientific and a commercial point of view, cholesteric liquid crystalline (LC) materials have always attracted considerable interest because of their unique optical-electric properties, including the selective reflection of light, thermochromism and circular dichroism. This has led to advanced applications such as nonlinear optical devices, full-colour thermal imaging, and organic pigment, etc. [1–17]. Chirality can be introduced into LC molecules at various levels, and is usually located in the terminal position of the mesogenic core. The chiral nematic phase is formed by rod-like, chiral molecules responsible for macroscopic alignment of cholesteric domains, depending on the chemical structures. For comb-like liquid crystalline polymers (LCP), their mesomorphism mainly depends on the nature of polymer backbone, the mesogenic units, the flexible spacer, and the nature of the terminal groups [18–22]. The polymer backbone and the mesogenic units have antagonistic tendencies: the polymer backbone is driven toward a random coil-type configuration, whereas the mesogenic units promote long-range orientational order. The mesogenic units are usually attached to the polymer backbone by a spacer. The spacer decouples the mesogenic side groups from the polymer backbone and enables the mesogenic units to order. Moreover, the backbones of side chain LCP reported are primarily polyacrylates, polymethacrylates and polysiloxanes. LCPs based on polyacrylates and polymethacrylates usually show higher viscosities. Therefore, a polysiloxane backbone and a spacer are chosen to obtain higher mobility of the mesophase, mesomorphism at moderate temperatures and higher thermal stability.

The aims of our research are: (a) to discuss the structure–property relationships of new chiral monomers and polymers based on cholesterol; and (b) to supply new chiral nematic compounds and necessary data to obtain piezoelectric LC networks by reacting these monomers with a nematic crosslinking agent. In a previous study, we reported the synthesis, structure and property of chiral LC polysiloxanes derived from menthol and (*S*)-(+)-2-methyl-1-butanol derivatives [23–26]. In this study, five new cholesteric monomers and their corresponding smectic polysiloxanes based on cholesteryl groups were prepared and characterised. These monomers based on cholesterol are effectively liquid crystal dimers, and there exists extensive literature on such materials [27–31]. The structures of these polymers are unusual and, in principle, similar materials have been reported by Yelamaggad and co-workers, i.e. dimers attached to a polymer backbone [32]. The phase behaviour of all LC monomers and polymers obtained was investigated with polarising optical microscopy (POM), differential scanning calorimetry (DSC), thermogravimetric analysis (TGA), and X-ray diffraction (XRD).

*Corresponding author. Email: hujs@mail.neu.edu.cn

ISSN 0267-8292 print/ISSN 1366-5855 online

DOI: 10.1080/02678292.2010.497229
http://www.informaworld.com

2. Experimental details

2.1 Materials

Hexanedioic acid was purchased from Shenyang Xinxi Reagent Co. (Shenyang, China). Cholesterol was purchased from Henan Xiayi Medical Co. (Xiayi, China). 4-Hydroxybenzoic acid was obtained from Shanghai Wulian Chemical Plant (Shanghai, China). Allyl bromide was purchased from Beijing Chemical Reagent Co. (Beijing, China). 4,4′-Dihydroxybiphenyl (from Aldrich) was used as received. Polymethylhydrosiloxane (PMHS, $\overline{M}_n = 700-800$) was purchased from Jilin Chemical Industry Co. (Jilin, China). Toluene used in the hydrosilylation reaction was purified by treatment with $LiAlH_4$ and distilled before use. All other solvents and reagents used were purified by standard methods.

2.2 Measurements

FT-IR spectra were measured on a PerkinElmer spectrum One (B) spectrometer (PerkinElmer, Foster City, CA). ^{1}H NMR spectra were obtained with a Bruker ARX400 spectrometer (Bruker, Swiss) in $CDCl_3$ solution using tetramethylsilane (TMS) as an internal reference. The elemental analyses were carried out with an Elementar Vario EL III (Elementar, Hanau, Germany). The specific optical rotations were obtained on a PerkinElmer 341 polarimeter. The thermal properties were determined with a Netzsch DSC 204 (Netzsch, Hanau, Germany) equipped with a cooling system. The heating and cooling rates were 10°C min^{-1}. The thermal stability of the polymers under nitrogen atmosphere was measured with a Netzsch TGA 209C thermogravimetric analyser. The heating rates were 20°C min^{-1}. A Leica DMRX POM (Leica, Germany) equipped with a Linkam THMSE-600 (Linkam, United Kingdom) cool and hot stage was used to observe the optical textures and phase transition temperatures. XRD measurements were performed with a nickel-filtered Cu-Kα radiation with a DMAX-3A Rigaku (Rigaku, Japan) powder diffractometer.

2.3 Synthesis of the intermediate compounds

The synthetic route of the intermediate compounds is outlined in Scheme 1. 4-Allyloxybenzoic acid (**6**), 4-allyloxy-4'-hydroxybiphenyl (**7**), 4-hydroxyphenyl-4'-allyloxybenzoate (**9**) and 4-hydroxybiphenyl-4'-allyloxybenzoate (**10**) were prepared according to the method reported previously [24, 33, 34].

2.4 6-Cholesteryloxy-6-oxohexanoic acid (2)

Hexanedioic acid (73.0 g, 0.5 mol), 120 mL of thionyl chloride and a few drops of dimethylformamide were reacted at room temperature for 2 h and 60°C for 5 h, then the excess thionyl chloride was removed under reduced pressure to give the corresponding acid chloride **1**. The solution of cholesterol (38.7 g, 0.1 mol) in 100 mL of chloroform and 8 mL of pyridine was added dropwise to the above compound **1** dissolved in 200 mL of chloroform under quick stirring. The mixture was reacted at room temperature for 2 h and refluxed for 15 h. After removing the solvent by rotary evaporator, the residue solid was poured into a beaker filled with 1000 mL of ice-water. This mixture was stirred for 1 h, filtrated, and the crude product was washed several times with warm water and ethanol, and then recrystallised from acetone. A solid **2** was obtained. Yield 67%, phase transition K137.0 (76.8)Ch148.3(4.0)I.

IR (KBr): 3250–2540 (–COOH); 2956, 2819 (CH3–, –CH2–); 1738, 1680 cm^{-1} (C=O).

^{1}H NMR ($CDCl_3$, TMS, δ): 0.75–2.61 [m, 51H, –(C***H***$_2$)$_4$– and cholesteryl–***H***]; 4.60 (m, 1H, –C***H***< in cholesteryl); 5.36 (d, 1H, >C=C***H***– in cholesteryl); 11.56 (s, 1H, –COO***H***).

2.5 4-(6-Cholesteryloxy-6-oxohexanoyloxy)benzoic acid (4)

6-Cholesteryloxy-6-oxohexanoyl chloride **3** was obtained through the reaction of the compound **2** with excess thionyl chloride according to the same method as for compound **1**. Compound **3** (26.6 g, 0.05 mol), dissolved in 15 mL of chloroform, was added dropwise to a solution of 4-hydroxybenzoic acid (8.3 g, 0.06 mol) in 100 mL of chloroform and 10 mL of pyridine under stirring. The mixture was reacted at room temperature for 2 h and refluxed for 15 h, and cooled to room temperature and then filtered. The concentrated filtrate was added to methanol, the crude product was washed several times with warm water and ethanol, and then recrystallised from ethanol/acetone (1:3). A solid **4** was obtained. Yield 73%, phase transition K152.9(15.1)Ch205.4(9.5)I.

IR (KBr): 3265–2549 (–COOH); 2949, 2868 (CH3–, –CH2–); 1761, 1734, 1691 (C=O), 1605–1466 cm^{-1} (Ar–).

^{1}H NMR ($CDCl_3$, TMS, δ): 0.72–2.63 [m, 51H, –(C***H***$_2$)$_4$– and cholesteryl–***H***]; 4.63 (t, 1H, –C***H***< in cholesteryl); 5.32 (d, 1H, >C=C***H***– in cholesteryl); 7.15–8.22 (m, 4H, Ar–***H***); 11.24 (s, 1H, –COO***H***).

2.6 Synthesis of the monomers

The synthetic route of the undecylenyl monomers is outlined in Scheme 2. The chiral monomers **M-1**–**M-5** were prepared by the same method. The synthesis of **M-1** is described below as an example.

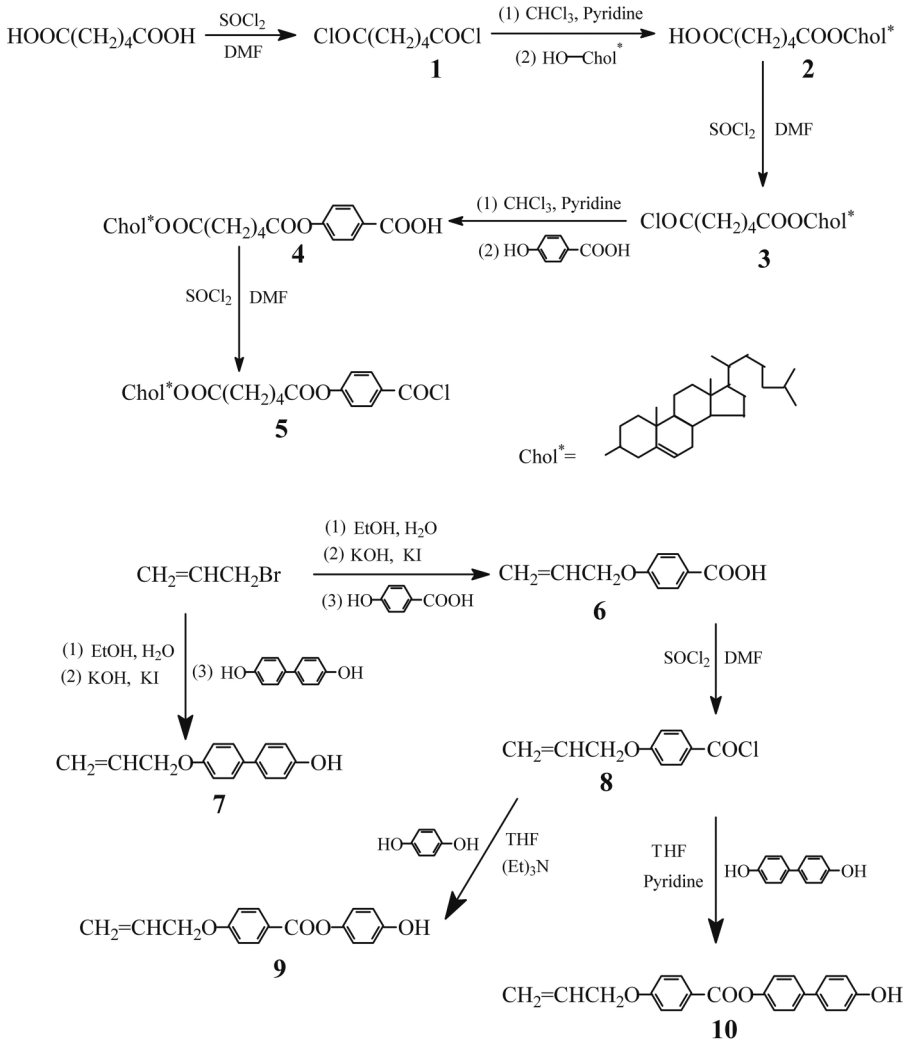

Scheme 1. Synthetic route of the intermediate compounds **1–10**.

2.6.1 4-Allyloxybiphenyl cholesteryl adipate (M-1)

The compound **3** (5.3 g, 0.01 mol), dissolved in 5 mL of chloroform, was added dropwise to a solution of the compound **7** (2.3 g, 0.01 mol) in 30 mL of chloroform and 0.8 mL of pyridine under stirring. The mixture was refluxed for 36 h, and then cooled to room temperature and then filtered. After the filtrate was concentrated, the crude product was precipitated by adding methanol to the filtrate, and recrystallised from $CHCl_3$/methanol (1:2). The solid was obtained. Yield: 65%.

IR (KBr): 3032 (=C–H); 2940, 2850 (CH3–, –CH2–); 1762, 1732 (C=O); 1650 (C=C); 1608–1496 (Ar–); 1252 cm^{-1} (C–O–C).

^{1}H NMR ($CDCl_3$, TMS, δ): 0.71–2.64 [m, 51H, –(C***H***$_2$)$_4$– and cholesteryl–***H***]; 4.66 (m, 3H, –C***H***$_2$O– and–C***H***< in cholesteryl); 5.35–5.50 (m, 3H, C***H***$_2$=CH and >C=C***H***– in cholesteryl); 6.03–6.11 (m, 1H, CH_2=C***H***–); 6.95–7.60 (m, 8H, Ar–***H***).

Elem. Anal. calcd for C48H66O5: C, 79.74; H, 9.20. Found: C, 78.82; H, 9.45.

2.6.2 4-(4-Allyloxybenzoyloxy)phenyl cholesteryl adipate (M-2)

Recrystallised from CHCl3/methanol (1:2). The solid was obtained. Yield: 54%.

IR (KBr): 3075 (=C–H); 2948, 2867 (CH3–, –CH2–); 1761, 1731 (C=O); 1649 (C=C); 1606–1510 (Ar–); 1253 cm^{-1} (C–O–C).

^{1}H NMR ($CDCl_3$, TMS, δ): 0.70–2.62 [m, 51H, –(C***H***$_2$)$_4$– and cholesteryl–***H***]; 4.65 (m, 3H, –C***H***$_2$O– and–C***H***< in cholesteryl); 5.34–5.50 (m, 3H, C***H***$_2$=CH and >C=C***H***– in cholesteryl); 6.05–6.14 (m, 1H, CH_2=C***H***–); 7.01–8.18 (m, 8H, Ar–***H***).

Elem. Anal. calcd for C49H66O7: C, 76.73; H, 8.67. Found: C, 77.20; H, 8.58.

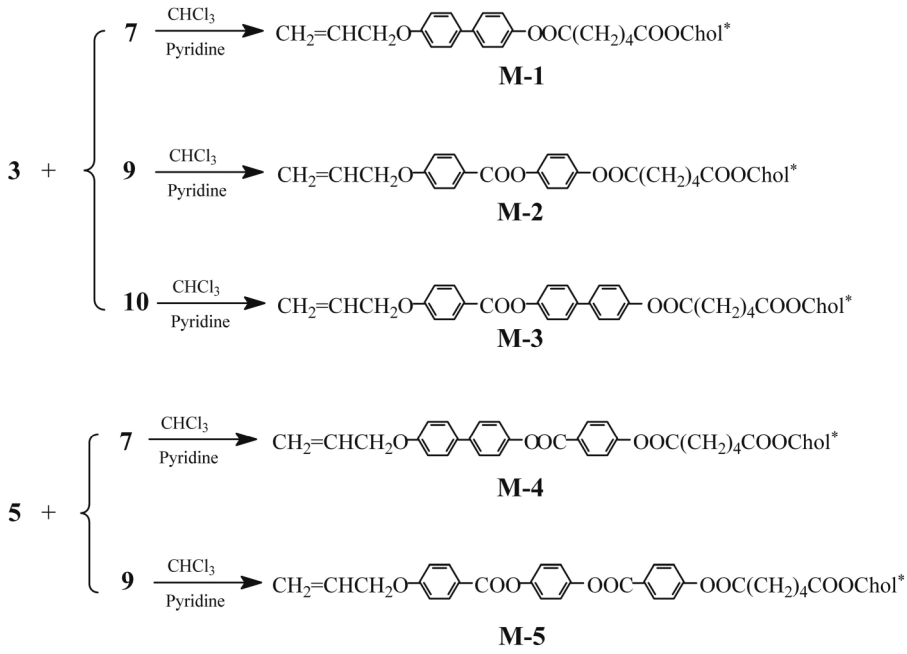

Scheme 2. Synthetic route of the monomers **M-1**–**M-5**.

2.6.3 4-(4-Allyloxybenzoyloxy)biphenyl cholesteryl adipate (M-3)

Recrystallised from $CHCl_3$/methanol (2:3). The solid was obtained. Yield: 50%.

IR (KBr): 3079 (=C–H); 2943, 2868 (CH3–, –CH2–); 1750, 1736 (C=O); 1650 (C=C); 1604–1493 (Ar–); 1255 cm^{-1} (C–O–C).

^1H NMR ($CDCl_3$, TMS, δ): 0.72–2.63 [m, 51H, –(CH_2)$_4$– and cholesteryl–***H***]; 4.62 (m, 3H, –C***H***$_2$O– and–C***H***< in cholesteryl); 5.32–5.53 (m, 3H, C***H***$_2$=CH and >C=C***H***– in cholesteryl); 6.02–6.12 (m, 1H, CH_2=C***H***–); 7.02–8.17 (m, 12H, Ar–***H***).

Elem. Anal. calcd for C55H70O7: C, 78.35; H, 8.37. Found: C, 78.70; H, 8.51.

2.6.4 4-((4-Allyloxybiphenyl-4'-yloxy)carbonyl) phenyl cholesteryl adipate (M-4)

Recrystallised from $CHCl_3$/methanol (2:3). The solid was obtained. Yield: 62%.

IR (KBr): 3079 (=C–H); 2946, 2867 (CH3–, –CH2–); 1757, 1734 (C=O); 1649 (C=C); 1604–1497 (Ar–); 1255 cm^{-1} (C–O–C).

^1H NMR ($CDCl_3$, TMS, δ): 0.70–2.61 [m, 51H, –(CH_2)$_4$– and cholesteryl–***H***]; 4.63 (m, 3H, –C***H***$_2$O– and–C***H***< in cholesteryl); 5.33–5.51 (m, 3H, C***H***$_2$=CH and >C=C***H***– in cholesteryl); 6.03–6.14 (m, 1H, CH_2=C***H***–); 6.96–8.28 (m, 12H, Ar–***H***).

Elem. Anal. calcd for C55H70O7: C, 78.35; H, 8.37. Found: C, 77.96; H, 8.48.

2.6.5 4-((4-(Allyloxybenzoyloxy)phenyl-4'-yloxy) carbonyl)phenyl cholesteryl adipate (M-5)

Recrystallised from $CHCl_3$/methanol (2:3). The solid was obtained. Yield: 65%.

IR (KBr): 3079 (=C–H); 2947, 2867 (CH3–, –CH2–); 1760, 1733 (C=O); 1648 (C=C); 1604–1509 (Ar–); 1256 cm^{-1} (C–O–C).

^1H NMR ($CDCl_3$, TMS, δ): 0.69–2.62 [m, 51H, –(CH_2)$_4$– and cholesteryl–***H***]; 4.65 (m, 3H, –C***H***$_2$O– and–C***H***< in cholesteryl); 5.32–5.52 (m, 3H, C***H***$_2$=CH and >C=C***H***– in cholesteryl); 6.04–6.13 (m, 1H, CH_2=C***H***–); 7.04–8.29 (m, 12H, Ar–***H***).

Elem. Anal. calcd for C56H70O9: C, 75.82; H, 7.95. Found: C, 76.22; H, 7.60.

2.7 Synthesis of the polymers

The synthetic route used to obtain the polymers **P-1**–**P-5** is outlined in Scheme 3. They were all prepared by the same method; the synthesis of **P-1** is described as a typical example. **M-1** (5 mol% excess versus the Si–H groups in PMHS) and PMHS were dissolved in dry toluene. The reaction mixture was heated to 65°C under nitrogen and anhydrous conditions, and then 2 mL of THF solution with the H_2PtCl_6 catalyst (5 mg mL^{-1}) was injected into the mixture with a syringe. The progress of the hydrosilylation reaction, monitored by the Si–H stretch intensity, went to completion, as indicated by IR. **P-1** was obtained by precipitation from toluene solution into

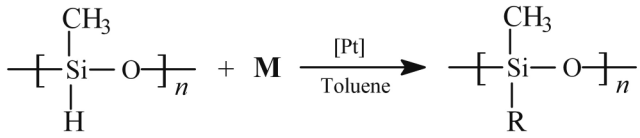

P-1, R= $CH_2CH_2CH_2O$ $OOC(CH_2)_4COOChol^*$

P-2, R= $CH_2CH_2CH_2O$ COO $OOC(CH_2)_4COOChol^*$

P-3, R= $CH_2CH_2CH_2O$ COO $OOC(CH_2)_4COOChol^*$

P-4, R= $CH_2CH_2CH_2O$ OOC $OOC(CH_2)_4COOChol^*$

P-5, R= $CH_2CH_2CH_2O$ COO OOC $OOC(CH_2)_4COOChol^*$

Scheme 3. Synthetic route of the polymers **P-1**–**P-5**.

methanol, purified by several filtrations from hot ethanol, and then dried in vacuum.

3. Results and discussion

3.1 Synthesis

The synthetic routes used to obtain **M-1**–**M-5** and **P-1**–**P-5** are shown in Schemes 2 and 3, respectively. Their chemical structures were characterised by FT-IR and ^{1}H NMR, and were in agreement with those expected. IR spectra of **M-1**–**M-5** showed characteristic stretching bands at about 1762-1750 cm^{-1} attributed to ester C=O linked to the cholesteryl group and 1736-1731 cm^{-1} attributed to ester C=O linked to an aromatic ring. ^{1}H NMR spectra of **M-1**–**M-5** showed multiplet at 8.29-6.95 and 6.14-5.32 ppm, corresponding to aromatic protons and olefinic protons in the allyl group, respectively. The polymers **P-1**–**P-5** were prepared through the hydrosilylation reaction using an excess amount of allyl monomers and PMHS. The unreacted monomer was removed by several reprecipitations from toluene solutions into methanol, and filtrations from hot ethanol. IR spectra of **P-1**–**P-5** showed the complete disappearance of the Si-H stretching band in PMHS at about 2165 cm^{-1} and olefinic C=C stretching band in the monomers at about 1650 cm^{-1}. Characteristic Si-C bands appeared at about 1260 and 798 cm^{-1}, and Si-O-Si bands appeared at about 1168, 1128 and 1031 cm^{-1}.

3.2 Specific optical rotations

The specific optical rotations of the monomers **M-1**–**M-5** and the corresponding polymers **P-1**–**P-5** were evaluated at 22°C in $CHCl_3$. The results are listed in Tables 1 and 2. The specific optical rotations of **M-1**–**M-5** and **P-1**–**P-5** were all left-handed, indicating that the configuration of these chiral new compounds is not apparently influenced by the series of chemical reaction. According to Table 1, the specific optical rotation values of the monomers having the same aryl numbers were essentially identical; however, they decreased with increasing the aryl number in the mesogenic core. Compared with the monomers **M-1** or **M-2** with two phenyl rings, **M-3**–**M-5** with more aryl segments (three phenyl rings) showed lower specific optical rotation values. The results suggest that the existence of highly conjugated biphenyl or higher phenyl segments affects the molecular polarity, leading to the decrease of the specific rotations.

Table 1. Specific optical rotation and thermal properties of monomers.

		Mesophase, phase transition temperature (°C) and enthalpy changes ($J \cdot g^{-1}$)	
Monomers	$[\alpha]_D^{22}$[a]	Heating cycle	Cooling cycle
M-1	−23.9	Cr 106(26.5)N*190(9.1)I	I169(1.3) N*–Cr
M-2	−22.8	Cr 133(42.9) N*193(14.6)I	I180(8.6) N*–Cr
M-3	−15.1	Cr 140(33.5)N*267(6.2)I	I199(0.9) N*–Cr
M-4	−15.7	g39(–) Cr 107(7.6) N*199(4.3)I	I199(0.4) N*–Cr
M-5	−15.3	g36(–) Cr 101(7.3) N*201(6.6)I	I200(0.5) N*–Cr

Notes: Cr = crystal; g = glass transition; N* = cholesteric phase; I = isotropic phase.
[a]specific optical rotation, 0.25 g in 100 mL of $CHCl_3$.

Table 2. Specific optical rotation, thermal properties and mesophase of polymers.

Polymer	$[\alpha]_D^{22}$[a]	Yield (%)	$\overline{M}_n$	T_g (°C)	T_i (°C)	ΔH ($J\ g^{-1}$)	T_d[c] (°C)	Mesophase
P-1	−18.7	94	8.0×10^3	40	200	9.9	292	SmA
P-2	−18.6	92	8.4×10^3	50	224	3.2	294	SmA
P-3	−11.5	93	9.2×10^3	59	276[b]	–	281	SmA
P-4	−12.2	90	9.1×10^3	53	210	6.9	285	SmA
P-5	−11.9	91	9.6×10^3	42	232[b]	–	280	SmA

Notes: [a]specific optical rotation, 0.15 g in 100 mL of $CHCl_3$.
[b]Temperature observed with POM.
[c]Temperature at which 5% weight loss occurred.
SmA = smectic A phase.

The specific optical rotation values of **P-1–P-5** showed the same tendencies as those described for the corresponding monomers. Moreover, the specific optical rotation values of **P-1–P-5** were less than those of the corresponding monomers. This indicates that the concentration of optically active sites decreases because these polymers consist of optically inactive polysilioxane. This affects the amount of optically active sites and leads to a decrease in the optical rotation.

3.3 Phase behaviour

The phase behaviour of the monomers **M-1–M-5** was investigated with DSC. Their phase transition temperatures and corresponding enthalpy changes, obtained on the second heating and cooling scans, are summarised in Table 1. Typical DSC curves of **M-2** are shown in Figure 1. DSC heating curves of **M-1–M-5** showed two endothermic peaks, which represent a melting transition at low temperature, and a chiral nematic to isotropic phase transition at high temperature, respectively. On cooling, only an isotropic to chiral nematic phase transition was seen, and crystallisation did not occur due to the supercooling of the samples. The clearing entropies are lower than might have been expected for structures of this type, and the usual explanation for this is the increase in molecular biaxiality given the bulky cholesteric group; similar effects have been described in the literature [35–38]. In addition, DSC heating curves of **M-4** and **M-5** also showed clear glass transition similar to the polymer.

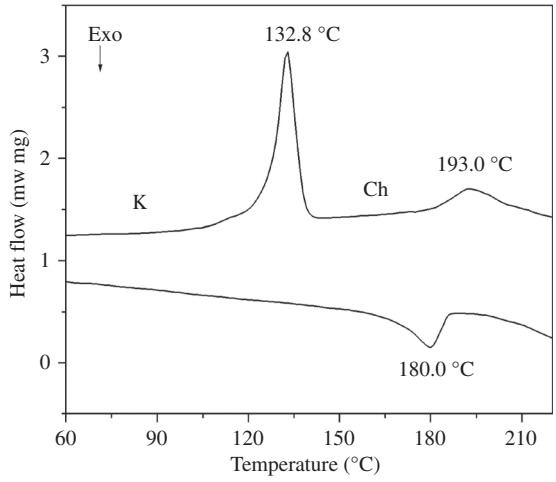

Figure 1. DSC curves of **M-2**.

The molecular structures had a considerable influence on the phase transition temperatures of **M-1**–**M-5**. In general, on increasing the number of aryl rings in the mesogenic core, the melting temperature (T_m) and the isotropic or clearing temperature (T_i) of the corresponding monomers also increased. For example, compared with T_m and T_i of **M-2**, those of **M-3** increased by 7°C and 74°C, respectively. Moreover, the mesophase temperature range widened from 60°C for **M-2** to 127°C for **M-3** because the increase of T_i was greater than that of T_m. Surprisingly, although the molecular structures of **M-4** and **M-5** were similar to those of **M-3**, namely their mesogenic cores contained three phenyl rings, their phase behaviour differed considerably, and T_m and T_i of **M-4** and **M-5** were less than those of **M-3**. In addition, **M-4** and **M-5**, respectively, also shows a glass transition.

The ester linking bond in the mesogenic core also had an influence on the phase transition temperatures, because the conjugation effect of the ester link makes T_m or T_i increase. According to Table 1, compared with the T_m and T_i of **M-1**, those of **M-2** increased by 27°C and 3°C, respectively.

In addition, although **M-2** and **M-3** were synthesised with the same chemical materials and method, and the molecular formula was also identical, their phase transition temperatures were different due to the different arrangement of their aryl mesogenic core or the change of the position of the biphenyl moiety in the mesogenic core. Specifically, (1) T_m of **M-3** was 140°C, while that of **M-4** was 107°C; (2) T_i of **M-3** was 267°C, while that of **M-4** was 199°C; (3) **M-4** also showed a glass transition at 39°C.

The phase behaviour of the polymers **P-1**–**P-5** was investigated with DSC, POM and TGA. The corresponding phase transition temperatures, thermal decomposition temperatures and mesophase types are summarised in Table 2. Representative DSC curves of **P-2** and **P-4** are presented in Figure 2. DSC curves showed a glass transition for **P-1**–**P-5** and LC to isotropic phase transition only for **P-1**, **P-2** and **P-4**. The DSC curves of **P-3** and **P-5** did not show obvious LC to isotropic phase transitions; however, POM results showed that **P-3** and **P-5** exhibited mesomorphism, so T_i of **P-3** and **P-5** was listed in Table 2 according to the POM results.

The glass transition temperature (T_g) and T_i of LC polymers are very important parameters in connection with structures and properties. For **P-1**–**P-5**, the nature of the mesogenic core affected their phase transition temperatures because they contain the same polysiloxane backbone, flexible spacer and terminal groups. According to Table 2, the effect of mesogenic units on T_g and T_i showed similar tendencies as those described for the corresponding monomers. In addition, the mesophase temperature ranges of **P-1**–**P-5** were greater than those of the corresponding monomers. This indicates that polymerisation can stabilise the LC phase, and widen the mesophase temperature ranges. Similar results and explanation have been reported elsewhere [39–41].

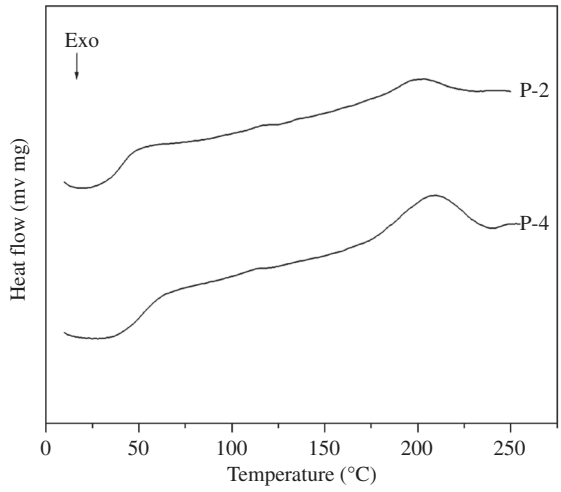

Figure 2. DSC curves of **P-2** and **P-4**.

The thermal stabilities of **P-1**–**P-5** were evaluated with TGA. The corresponding data are shown in Table 2. The weight decreased by 40–48% when the temperature increased to 400°C; this is due to the occurrence of the thermal degradation of the mesogenic units in side groups. Moreover, TGA results showed that the temperatures at which 5% weight loss occurred (T_d) were greater than 280°C for **P-1**–**P-5**; this indicates that all the polymers had good thermal stabilities.

3.4 Optical textures

In general, chiral LC materials show the chiral nematic phase. At zero field this exhibits two optically contrasting stable states: planar (including oily streak and finger print) and focal conic textures. When the chiral nematic phase is in the planar state, the helical axis is perpendicular to the cell surface; when it is in the focal conic state, the helical axis is more or less parallel to the cell surface.

POM results showed that **M-1**–**M-5** all exhibited enantiotropic oily streak textures on heating and focal conic textures on cooling; moreover, the focal conic texture easily transformed to oily steak texture by shearing the mesophase. In addition, **M-1** and **M-5** also exhibited cholesteric finger print texture. The optical micrographs of **M-1**, **M-2** and **M-4** are shown in Figure 3. **P-1**–**P-5** exhibited a batonnet or fan-shaped texture of a smectic A (SmA) phase; in this

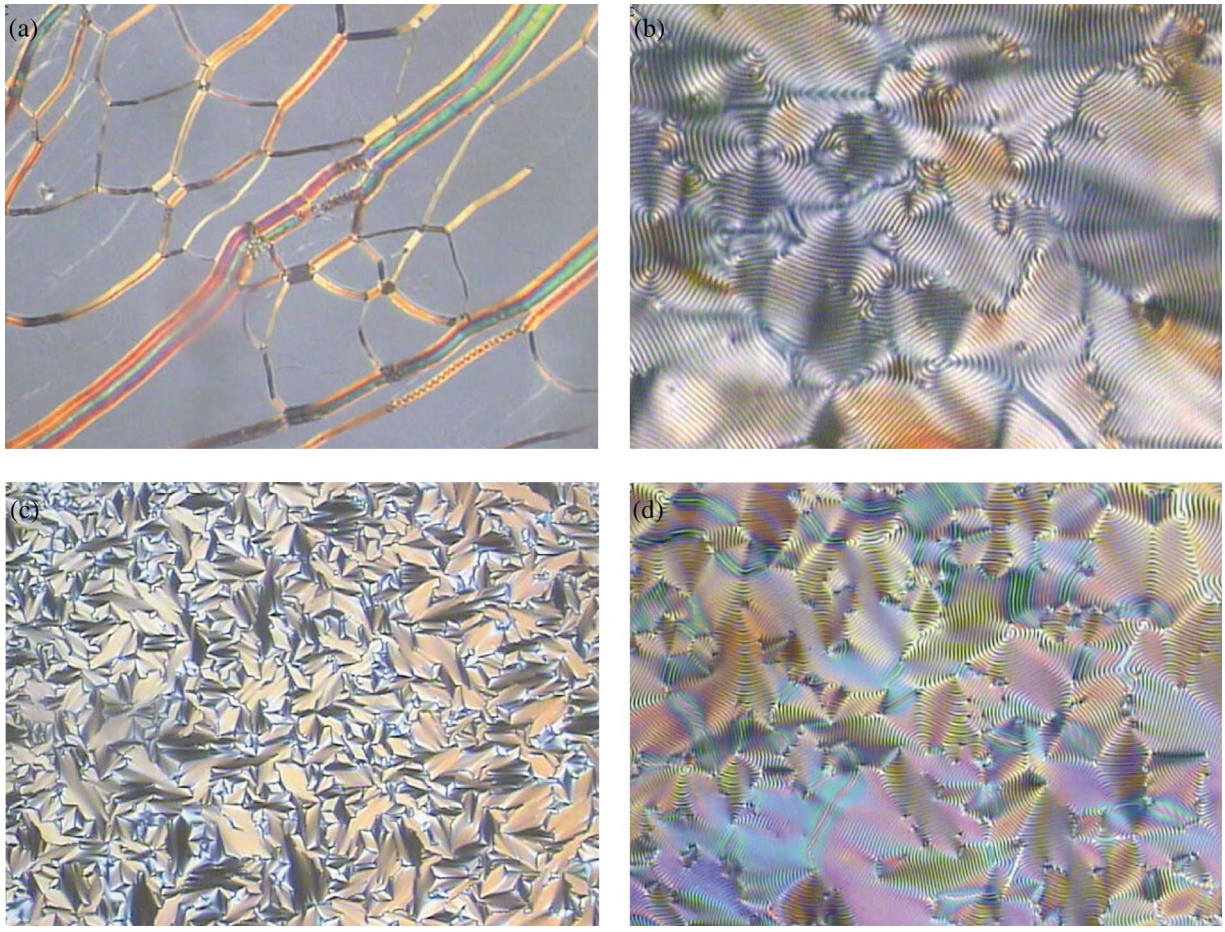

Figure 3. Optical textures of monomers (200×). (a) Oily streak texture on heating to 165°C for **M-1**; (b) finger print texture on heating to 188°C for **M-1**; (c) focal conic texture on cooling to 155°C for **M-2**; (d) oily streak texture on heating to 137°C for **M-4**.

case the smectic layers are basically perpendicular to the substrate plane. The optical micrograph of **P-2** is shown in Figure 4. Although **M-1**–**M-5** exhibited the chiral nematic phase, the corresponding polymers **P-1**–**P-5** only displayed a SmA phase. This indicates that the polymer chains hinder the formation of the helical supramolecular structure of the mesogenic units, and the mesogenic moieties are ordered in a smectic arrangement with their centres of gravity in layers. Moreover, the mesophase formed by side chain LCPs is more organised than that exhibited by the corresponding monomers based on cholesterol.

3.5 XRD analysis

XRD studies were carried out to obtain more detailed mesophase type. In general, a sharp peak associated with the smectic layers at small angle ($2\theta < 5°$) and a broad peak associated with the lateral packings at wide angle can be observed for smectic phase structure. For **P-1**–**P-5**, their X-ray patterns exhibited a sharp reflection at $3.2 < 2\theta < 2.5°$, the *d*-spacing of the first-order

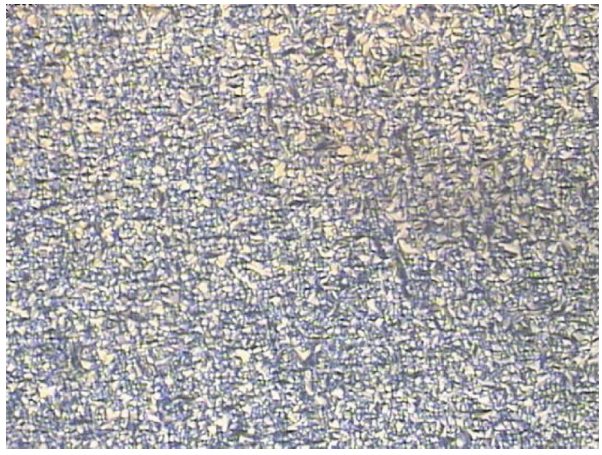

Figure 4. Fan-shaped texture of a SmA phase at 184°C for **P-2** (200×).

reflections was 27.6 ~ 35.3 Å. Moreover, the *d*-spacing of the first-order reflection hardly changed with temperature. This provides strong evidence for the formation of the SmA phase. Figure 5 shows the XRD curves

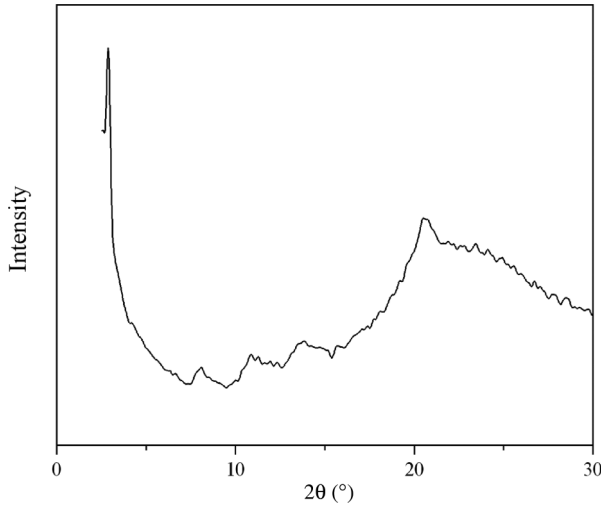

Figure 5. XRD curves of **P-2**.

of **P-2** at mesophase as an example. The corresponding reflection angle and *d*-spacing of the first-order reflection were 2.9° and 30.4 Å, respectively.

4. Conclusions

Five new cholesteric monomers and their corresponding side-chain smectic polymers were synthesised and characterised. These monomers and polymers with more aryl segments showed lower specific optical rotation values. The monomers **M-1**–**M-5** showed typical chiral nematic phase, and the polymers **P-1**–**P-7** exhibited the SmA phase. This indicates that the polymer chains hinder the formation of the helical supermolecular structure. In addition, this behaviour is attributed to an increased molecular weight and density of the mesogenic units in side chain, and hence a more ordered organisation in the LC phases. Moreover, T_m or T_g and T_i increased, and mesophase temperature ranges widened with increasing the aryl number in the mesogenic core. The mesophase temperature ranges of **P-1**–**P-5** were greater than those of the corresponding monomers. All of the homopolymers obtained displayed very good thermal stability.

Acknowledgements

The authors are grateful to National Natural Science Foundation of China (No. 50503005) and Fundamental Research Funds for the Central Universities (No. N090505002) for financial support of this work.

References

[1] Broer, D.J.; Lub, J.; Mol, G.N. *Nature (London, UK)* **1995**, *378*, 467–469.
[2] Hsiue, G.H.; Lee, R.H.; Jeng, R. *J. Polymer* **1997**, *38*, 887–895.
[3] Palffy-Muhoray, P. *Nature (London, UK)* **1998**, *391*, 745.
[4] Bobrovsky, A.Y.; Boiko, N.I.; Shaumburg, K.; Shibaev, V.P. *Liq. Cryst.* **2000**, *27*, 1381–1387.
[5] Watanabe, J.; Kamee, H.; Fujiki, M. *Polym. J.* **2001**, *33*, 495–497.
[6] Hu, J.S.; Zhang, B.Y.; Liu, Z.J.; Zang, B.L. *J. Appl. Polym. Sci.* **2002**, *86*, 2670–2676.
[7] Shibaev, P.V.; Kopp, V.I.; Genack, A.Z. *J. Phys. Chem. B* **2003**, *107*, 6961–6964.
[8] Ogawa, H.; Stibal-Fischer, E.; Finkelmann, H. *Macromol. Chem. Phys.* **2004**, *205*, 593–599.
[9] Hamley, I.W.; Castelletto, V.; Parras, P.; Lu, Z.B.; Imrie, C.T.; Itoh, T. *Soft Matter* **2005**, *1*, 355–363.
[10] Hartwig, A.; Mahato, T.K.; Kaese, T.; Wöhrle, D. *Macromol. Chem. Phys.* **2005**, *206*, 1718–1730.
[11] Ohta, R.; Togashi, F.; Goto, H. *Macromolecules* **2007**, *40*, 5228–5230.
[12] Xing, X.J.; Baskaran, A. *Phys. Rev. E: Stat., Nonlinear, Soft Matter Phys.* **2008**, *78*, 021709 1–7.
[13] Guo, J.; Sun, J.; Li, K.; Cao, H.; Yang, H. *Liq. Cryst.* **2008**, *35*, 87–97.
[14] Aldred, M.P.; Hudson, R.; Kitney, S.P.; Vlachos, P.; Liedtke, A.; Woon, K.L.; Kelly, S.M. *Liq. Cryst.* **2008**, *35*, 413–427.
[15] Gupta, V.K.; Sharma, R.K.; Mathews, M.; Yelamaggad, C.V. *Liq. Cryst.* **2009**, *36*, 339–343.
[16] Cong, Y.H.; Wang, W.; Tian, M.; Meng, F.B.; Zhang, B.Y. *Liq. Cryst.* **2009**, *36*, 455–460.
[17] Zhan, X.; Jing, X.; Wu, C. *Liq. Cryst.* **2009**, *36*, 1349–1354.
[18] Le Barney, P.; Dubois, J.C.; Friedrich, C.; Noel, C. *Polym. Bull.* **1986**, *15*, 341–348.
[19] Hsu, C.S.; Percec, V. *J. Polym. Sci. Polym. Chem. Ed.* **1989**, *27*, 453–459.
[20] Hsiech, C.J.; Wu, S.H.; Hsiue, G.H.; Hsu, C.S. *J. Polym. Sci. Part A: Polym. Chem.* **1994**, *32*, 1077–1085.
[21] Wu, Y.H.; Lu, Y.H.; Hsu, C.S. *J. Macromol. Sci., Part A: Pure Appl. Chem.* **1995**, *A32*, 1471–1488.
[22] Soltysiak, J.T.; Czupryński, K.; Drzewiński, W. *Polym. Int.* **2006**, *55*, 273–278.
[23] Hu, J.S.; Zhao, Z.X.; Kong, B.; Li, D. *Colloid Polym. Sci.* **2009**, *287*, 215–224.
[24] Zhang, B.Y.; Hu, J.S.; Ren, S.C.; Liu, C. *J. Appl. Polym. Sci.* **2009**, *111*, 3016–3025.
[25] Hu, J.S.; Wei, K.Q.; Zhang, B.Y.; Yang, L.Q. *Liq. Cryst.* **2008**, *35*, 925–935.
[26] Zhang, B.Y.; Hu, J.S.; Yang, L.Q.; He, X.Z.; Liu, C. *Euro. Polym. J.* **2007**, *43*, 2017–2027.
[27] Goodby, J.W.; Saez, I.M.; Cowling, S.J.; Gasowska, J.S.; MacDonald, R.A.; Sia, S.; Watson, P.; Toyne, K.J.; Hird, M.; Lewis, R.A.; Lee, S.E.; Vaschenko, V. *Liq. Cryst.* **2009**, *36*, 567–605.
[28] Imrie, C.T.; Henderson, P.A. *Curr. Opin. Colloid Interface Sci.* **2002**, *7*, 298–311.
[29] Imrie, C.T.; Henderson, P.A. *Chem. Soc. Rev.* **2007**, *36*, 2096–2124.
[30] Imrie, C.T.; Henderson, P.A.; Yeap, G.Y. *Liq. Cryst.* **2009**, *36*, 755–777.
[31] Yelamaggad, C.V.; Shanker, G.; Hiremath, U.S.; Prasad, S.K. *J. Mater. Chem.* **2008**, *18*, 2927–2949.
[32] Lee, J.W.; Oh, D.K.; Yelamaggad, C.V.; Nagamani, S.A.; Jin, J.I. *J. Mater. Chem.* **2002**, *12*, 2225–2230.
[33] Hu, J.S.; Zhang, B.Y.; Feng, Z.L.; Wang, H.G.; Zhou, A.J. *J. Appl. Polym. Sci.* **2001**, *80*, 2335–2340.

[34] Hu, J.S.; Ren, S.C.; Zhang, B.Y.; Chao, C.Y. *J. Appl. Polym. Sci.* **2008**, *109*, 2187–2194.
[35] Yeap, G.Y.; Hng, T.C.; Yeap, S.Y.; Gorecka, E.; Ito, M.M.; Ueno, K.; Okamoto, M.; Mahmood, W.A.K.; Imrie, C.T. *Liq. Cryst.* **2009**, *36*, 1431–1441.
[36] Imrie, C.T. *Liq. Cryst.* **1989**, *6*, 391–396.
[37] Attard, G.S.; Imrie, C.T. *Liq. Cryst.* **1992**, *11*, 785–789.
[38] Attard, G.S.; Imrie, C.T.; Karasz, F.E. *Chem. Mater.* **1992**, *4*, 1246–1253.
[39] Craig, A.A.; Imrie, C.T. *Macromolecules* **1999**, *32*, 6215–6220.
[40] Craig, A.A.; Imrie, C.T. *Macromolecules* **1995**, *28*, 3617–3624.
[41] Imrie, C.T.; Karasz, F.E.; Attard, G.S. *Macromolecules* **1993**, *26*, 3803–3810.